Azimuthal Instabilities of an Annular Combustor with Different Swirling Injectors

Preethi Rajendram Soundararajan, Daniel Durox, Antoine Renaud, Sébastien Candel

GT2022-82281

DRAFT: AZIMUTHAL INSTABILITIES OF AN ANNULAR COMBUSTOR WITH DIFFERENT SWIRLING INJECTORS

Preethi Rajendram Soundararajan [1]*, Daniel Durox [1], Antoine Renaud [1], Sébastien Candel [1]

[1]Laboratoire EM2C, CNRS, CentraleSupélec, Université Paris-Saclay, 3, rue Joliot Curie, 91192 Gif-sur-Yvette cedex, France
Email: preethi.rajendram-soundararajan@centralesupelec.fr

ABSTRACT

Experiments are carried out on the laboratory-scale MICCA-Spray annular combustor to examine the effects of swirlers on combustion instabilities. The system comprises sixteen spray-swirl injectors and gives rise to instabilities coupled by azimuthal modes. Five types of swirlers producing clockwise rotation and varying in swirl numbers and pressure drops are considered. These swirlers can be broadly categorized into two groups, lower-swirl, and higher-swirl groups, based on their swirl numbers. Additionally, an alternate arrangement of clockwise and counterclockwise swirlers is also studied. Experiments are performed systematically with liquid heptane at five levels of thermal power and six equivalence ratios. Results reveal that none of the swirlers in the lower-swirl category exhibit instability in the operating region considered, whereas the higher-swirl units feature strong azimuthal instabilities that are quasi-limit cycle with a few short and random bursts. Among the higher-swirl group, a higher pressure drop swirler is associated with a broader instability map. This shows that the transition to instability mainly depends on the swirl number through its effect on the flame structure and that the pressure drop adds to further variations in amplitude and frequency of oscillation. The spin ratio time series indicate that the modes are of mixed type, and that their distribution depends on the operating condition. On specifically comparing the spin ratio distribution between a full set of co-rotating swirlers (CR) and a configuration where co- and counter-rotating swirlers (CCR) are alternatively placed, it is found that there is no definite statistical preference for spin ratio due to the effect of bulk swirl. In some cases, however, the CCR configuration promotes a broader distribution of spin ratios centered around the standing mode ($s = 0$) while the CR setup favors azimuthal modes spinning in the counterclockwise direction. An attempt is made to interpret the data by making use of flame describing functions (FDFs) measured in a single-injector combustor. It is found that the FDFs corresponding to the two swirler categories are relatively distinct. Using a low-order model in which the injector is represented by its impedance and considering that this impedance shifts the band of instability, it is tentatively proposed that the unstable behavior may be linked to the relative position of the FDF phase with respect to the instability boundary in the frequency range corresponding to the expected azimuthal mode frequency and to differences in the FDF gains.

Keywords: Annular combustor, Azimuthal instabilities, Spray flame, Swirl injector, Flame describing function.

1 INTRODUCTION

Combustion instabilities have been the subject of an intense research effort [1, 2] with much of the more recent work focused on gas turbine applications. In these systems the combustor geometry is mostly annular and the coupling modes are predominently azimuthal [3]. It is generally considered that these modes are the most dangerous because they are less well damped and also because they correspond to the lowest eigenfrequencies where flames are most sensitive to disturbances. These azimuthal modes in turn induce axial velocity fluctuations in each injec-

*Address all correspondence to this author.

tor [4], a process which dominantly leads to heat release rate fluctutations. Experiments carried out on lab-scale and industrial annular combustors [5–8], numerical simulations [4,9–12], and theoretical analysis [13, 14] have provided a wealth of information on azimuthal coupling. Other investigations aim at developing active and passive control techniques [15–18] for reducing such instabilities. This article is specifically concerned with effects related to the swirling injector. The injector unit [19, 20] is known to determine the flame structure and dynamical characteristics, and it is important to document its influence on azimuthal combustion instabilities. This could help unravel the mechanisms of instabilities associated with swirling injectors and might in turn help identify injector architectures that are less sensitive to disturbances and less prone to instabilities.

Before moving further, it is worth considering some of the past research efforts carried out on annular combustors and the influence of swirler on acoustic instabilities to give a context for the present work and identify the existing knowledge gap. A large eddy simulation (LES) of a full aeronautical combustor was carried out in [10] to capture the azimuthal modes of this combustor. Results revealed that the amplitude of azimuthal modes vary with time, resulting in pressure fluctuations changing between purely standing and spinning modes. It was also identified that the presence of a bulk swirling convection velocity resulted in slow rotation of the standing mode. The effect of injector spacing on instabilities was analyzed in [5, 21] on an annular combustor with flames stabilized by a bluff-body. The time evolution of the pressure variations indicated constant switching between standing and spinning modes similar to [10]. It was found that for larger separation distances between injectors, each flame unit behaved independently and adopted a helical structure of heat release rate. Additionally, the effect of bulk swirl motion on instabilities was investigated in [5]. The configuration with alternating swirl directions resulted in statistically preferred standing modes while for the arrangement where all swirlers rotated in the same direction, the statistical preference depended on the operating conditions considered. The direction of spin dominantly depended on the bulk swirl direction. Early studies were carried out with matrix burners in the lab-scale annular combustor MICCA. Several pure azimuthal modes, such as standing, spinning [22], and slanted [23] modes were observed in this system. Experiments were also carried out on this combustor to identify the effect of symmetry breaking by partially blocking the injectors or changing their geometry [8].

At this point, it is also useful to identify the role of the injection units in the mechanism leading to combustion instabilities. Several studies indicate the presence of a strong interaction between the flow behavior in a swirl combustor and combustion instability (for example [24]). This reveals a possibility of developing control techniques by altering the flow structures [25] through modification of swirler geometry. Few researchers have have pursued this, but such studies are limited only to simplified single burner test rigs. For example, the effect of inlet swirl number was studied in [26] using LES and it was observed that strong swirling flows resulted in transverse acoustic oscillations whereas with weak swirls longitudinal instabilities prevailed. Komarek et al. [27] attempted to identify the effect of swirl number fluctuations by varying the axial position of the swirl generator. Through the combination of experiments and numerical simulations, it was identified that the position of the swirl generator had a strong impact on the flame's dynamical response. Another study that considered the effect of swirler number was reported in [28]. Two swirl numbers were experimentally studied and it was observed that the normalized pressure and heat release rate oscillations were more intense in the stronger swirl number case compared to the weaker swirl configuration. Recently, Zhang et al. [29] performed LES on a premixed swirl-stabilized combustor and found changes in the zones of instability depending on the swirl number value. It was identified that the corner recirculation zones played a major role in inducing heat release rate fluctuations compared to the central recirculation zone. Apart from the dependence on swirl number, the work carried out in [30] revealed the effect of swirler pressure drop on combustion instabilities. A recent study by the same authors [31] in a single-injector combustor has shown that the longitudinal self-sustained instabilities strongly depend on the swirler type used. A low-order model based on injector impedance using flame describing function (FDFs) was also shown to predict these instabilities. FDFs from single-injector systems have also been used to successfully predict instabilities of annular combustors equipped with matrix burners featuring laminar flames [12]. But the predictions are less precise in [7] as the specific dynamics of spray-swirl injectors were not considered.

The above review shows that the swirler effect on instabilities has been investigated in single-injector combustors, but such studies have not been carried out in annular combustors to our knowledge. The current investigation would thus help in bridging several knowledge gaps. (1) What happens when the swirl number and pressure drop of the injector unit are systematically varied in an annular combustor? Such knowledge would help develop swirlers that are less susceptible to instabilities. (2) What happens to the modal structure in a configuration where alternate co- and counter-rotating swirlers are placed compared to a configuration where all the swirlers are co-rotating? (3) Can a simplified single-injector setup capture some of the features exhibited by the multi-flame annular combustor where there are flame-flame interactions?

To answer the above questions, the current experimental investigation presents systematic documentation of instabilities observed in the lab-scale MICCA-Spray annular combustor. The experimental setup is presented in Section 2. The stability map of the annular combustor with the various swirler configurations is presented in Section 3 followed by a discussion of the modal structure between a fully co-rotating configuration and an alter-

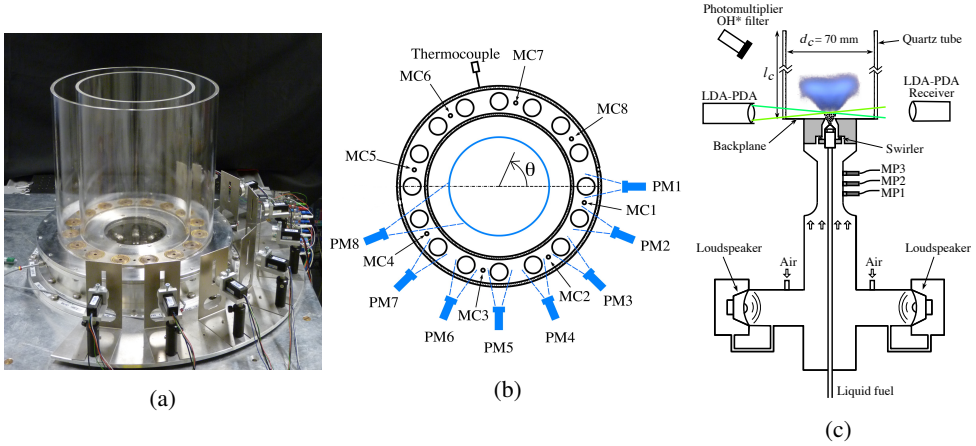

(a) (b) (c)

FIGURE 1: (a) Photograph of the MICCA-Spray setup. The height of the combustion chamber is maintained at 400 mm for both the inner and the outer chamber walls. (b) Schematic top view of the combustion chamber showing the locations of chamber microphones (MCx) and photomultipliers (PMx). The azimuthal angle θ is positive along the counterclockwise direction and its baseline is taken along the centreline of injector 1. Adapted from [7, 32]. (c) Schematic diagram of complementary single-injector setup SICCA-Spray.

nate co- and counter-rotating configuration in Section 4. The results from a complementary single-injector setup, SICCA-Spray, with the various swirlers are finally presented in Section 5, along with a discussion on how they can help analyze the instabilities observed in the annular system.

2 EXPERIMENTAL SETUP OF MICCA-SPRAY

The experimental setup of the lab-scale annular combustor MICCA-Spray is shown in Fig. 1(a) & (b). Only the main features of the test rig are described here, and the readers are referred to [7] for a more detailed description. The test rig consists of an annular plenum connected to the annular combustion chamber through sixteen swirling injectors. The injectors consist of an air distributor which supplies air from the plenum to the swirler followed by a terminal plate having a conical section with 8 mm outlet diameter. These injectors feature a high value of swirl number and abrupt area changes resulting in strong pressure drops across the swirler, thus making them only weakly transparent to acoustic waves. In the present study, liquid heptane is used as fuel and is delivered into the chamber through a simplex atomizer mounted on the injector. The atomizer disperses finely atomized fuel droplets into the chamber as a hollow cone spray in the presence of air flow. The chamber of the MICCA-Spray consists of two concentric, cylindrical quartz tubes of height 400 mm. The inner wall has an outer diameter of 300 mm and the outer wall has an inner diameter of 400 mm resulting in mean diameter of 350 mm. Air flow rate is controlled through a Bronkhorst EL-FLOW mass flow meter, which has a relative accurancy of 0.6%, and the fuel flow rate is controlled by a Bronkhorst CORI-FLOW controller, which has a relative accuracy of 0.2%. Eight Brüel & Kjær microphones are mounted on the chamber (marked as MCx in Fig. 1(b)). These microphones are placed on waveguides whose ports are flush-mounted on the chamber backplane to prevent direct contact of the microphones with the hot chamber environment. The waveguide ports are located between every two injectors, and they are terminated by a 25 m long tube to prevent any wave reflections. The microphone measurements are acquired at a sampling frequency of $f_s = 32\,768$ Hz for a total time period of $T_0 = 16$ s. Additionally, the chamber is equipped with eight photomultipliers to capture the light intensity fluctuations, but the result of these measurements are not discussed here.

For the present study, five different radial swirlers with six tangential channels are tested. The swirlers are named 707, 712, 716, 726, and 727, and their characteristics are provided in Tab. 1. The geometrical parameters of the swirlers are represented in terms of d_{sc}, which is the diameter of the swirler channels, and $R_{0,sc}$ which is the radial distance between the axis of a channel and the axis of the swirler. These two geometrical parameters are suitably varied to obtain different swirl numbers S_N and pressure drops Δp. The swirlers can be grouped into two categories based on their swirl number: the lower-swirl category comprising swirlers 707 and 712, and the higher-swirl category comprising the rest of the swirlers. Each group also contains swirlers with the same swirl number values but different pressure drops. The swirlers 707 and 712 have almost the same swirl number but different pressure drop values. Their swirl number is lower than the swirler numbers of the higher-swirl category. Among the higher-swirl category, the swirlers 726 and 727 have the same swirl numbers but a slightly different pressure drop, while the swirlers 716 and 727 have almost the same pressure

TABLE 1: Swirler characteristics measured under cold flow at an air flow rate of $\dot{m}_{\text{air}} = 2.6\,\text{g s}^{-1}$ and 2.5 mm above chamber backplane. Δp represents the pressure drop of the injector and S_N represents the experimentally obtained swirl number. d_{sc} is the diameter of the swirler channels and $R_{0,sc}$ is the distance between the axis of a channel and the axis of the swirler.

Category	Swirler (-)	S_N (-)	Δp (kPa)	σ (-)	d_{sc} (mm)	$R_{0,sc}$ (mm)
Lower-swirl	707	0.60	3.65	3.33	4.0	4.6
	712	0.59	4.50	4.10	3.0	2.3
Higher-swirl	716/816	0.70	5.74	5.23	3.5	4.7
	726	0.74	6.00	5.47	3.5	5.5
	727	0.74	5.70	5.20	3.5	5.1

drop, but 727 has a higher swirl number. In addition to the five swirling injectors, a combination of co-rotating (716-type) and counter-rotating (namely, 816) swirlers are placed alternatively to understand the effect of overall mean swirl on instabilities. Swirler 816 is completely identical to the swirler 716 except in the swirl direction.

3 STABILITY MAP OF MICCA-SPRAY ANNULAR COMBUSTOR

The stability map of MICCA-Spray annular combustor is obtained by performing measurements at five levels of thermal power $\mathcal{P}$ and, at each level, six different equivalence ratios ϕ are tested, resulting in a total of thirty operating points per swirler. At each operating point, the fuel flow rate is fixed, and the air flow rate is systematically varied to obtain different equivalence ratios. The stability map of MICCA-Spray is represented in terms of two parameters, amplitude and frequency of instability, to suitably represent the first azimuthal-first longitudinal 1A1L azimuthal modes exhibited in the assessed operating points. Considering a $e^{-i\omega t}$ sign convention for the acoustic waves, at any instant t, the acoustic pressure measured by the chamber microphones can be represented as:

$$p'_c(\theta,t) = A^+ \exp(i\theta - i\omega t) + A^- \exp(-i\theta - i\omega t) \qquad (1)$$

In the above equation, p'_c represents the instantaneous pressure measured by the microphones, A^+ and A^- represent counterclockwise and clockwise spinning waves respectively of the 1A1L mode, and θ is the azimuthal angle which is considered positive along the counterclockwise direction. The instantaneous measurements from the eight chamber microphones provide the possibility to obtain an indicator of instability that is spatially averaged over the annulus and temporally averaged over the duration of acquisition [7]. This amplitude $\mathcal{A} = (|A^+|^2 + |A^-|^2)^{1/2}$ is proportional to the root mean square (RMS) amplitude and is independent of the structure of the unstable mode. $\mathcal{A}$ is used to compare the instability between the different swirlers along with the instability frequency f_i, which is the peak frequency from the power spectrum of the microphone signals. The microphone signals are bandpass-filtered between 500 Hz and 1100 Hz and the time-resolved analytical signals are obtained through Hilbert transform. The wave amplitudes are then reconstructed up to the third order in azimuthal harmonics [32]. In addition to comparing the amplitude and frequency of instability, the spin ratio s_r is calculated to identify the structure of the azimuthal instabilities and is given by,

$$s_r = \frac{|A^+| - |A^-|}{|A^+| + |A^-|} \qquad (2)$$

$s_r = 1$ represents a counterclockwise spinning wave, $s_r = -1$ represents a clockwise spinning wave, and $s_r = 0$ corresponds to a standing azimuthal wave.

The behavior of the swirlers in the lower-swirl category (707 and 712) is peculiar as they do not exhibit any azimuthal instability for the operating points assessed, and the amplitude of the pressure fluctuation signals always remains below 50 Pa. On the contrary, all the swirlers in the higher-swirl category exhibit an unstable behavior. Although the various swirlers have similar geometries, a minor change resulting in the reduction of swirl number improves the stability of the annular combustor. This study therefore highlights a critical value $S_{Ncrit} < 0.7$ for the swirl number in order to have unconditional stability for the studied operating points. For the different swirlers in the higher swirl category, stability maps representing the amplitude and frequency of instability are shown in Fig. 2. The data obtained at the thirty operating points are interpolated to derive the stability maps shown in the figure.

A previous study by the same authors [7] reported the results of swirler 716 to identify the effect of fuel type on combustion instabilities. These results are reproduced in this article to facilitate comparison with other swirlers. Overall, the swirlers exhibit gradual changes from stable to unstable states as the operating point are varied. On comparing the three swirlers in the higher-swirl category (716, 726, 727), the highest amplitude of instability is exhibited by swirler 716 ($\mathcal{A}_{\max} \approx 1673$ Pa) at $\mathcal{P} = 110$ kW at slightly fuel-rich conditions ($\phi = 1.05$). This is followed by swirler 727 which exhibit a maximum amplitude of $\mathcal{A}_{\max} \approx 1540$ Pa at $\mathcal{P} = 118$ kW, also in slightly rich conditions, and then swirler 726 which reaches the maximum amplitude of $\mathcal{A}_{\max} \approx 1460$ kPa at both $\mathcal{P} = 118$ and 110 kW in slightly rich

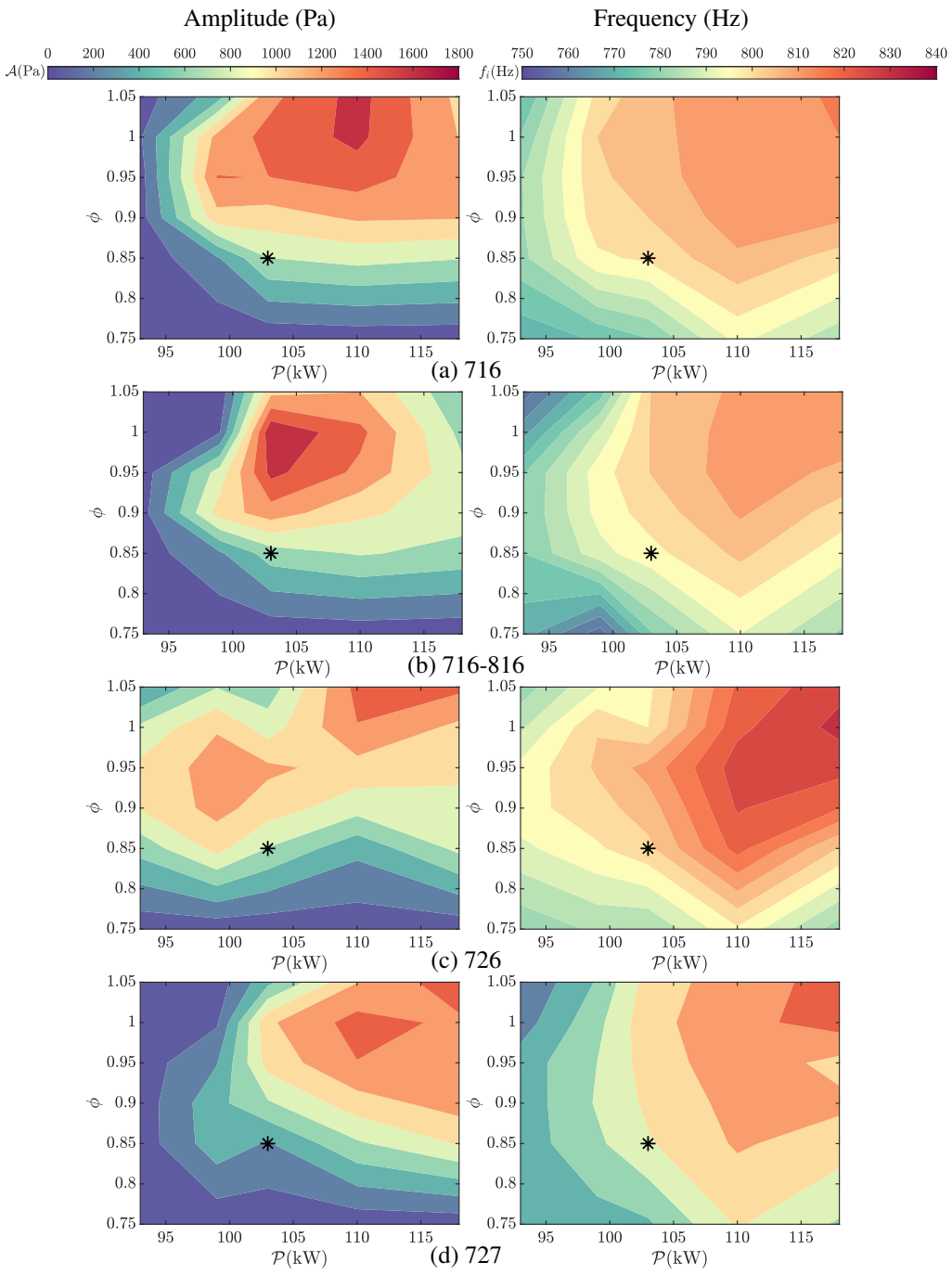

FIGURE 2: Amplitude (left) and frequency (right) stability map of MICCA-Spray for the different swirlers in higher-swirl category. The swirlers in the lower-swirl category (707 and 712) are always stable in the assessed operating zone and hence are not shown here. The black star on the stability map refers to the operating conditions of the complementary single-injector combustor described in Section 5.

conditions. The amplitude stability map of 727 evolves similar to 716 (Fig 2(a) & (d) left), while it differs from the map of 726, which has the broadest instability region among the three swirlers, exhibiting instability even at the lowest power. The swirlers 727 and 716 possess the same pressure drop, which is slightly lower than the pressure drop of 726. This observation points to the dependence of instability amplitude on the pressure drop; a higher pressure drop for the same swirl number appears to

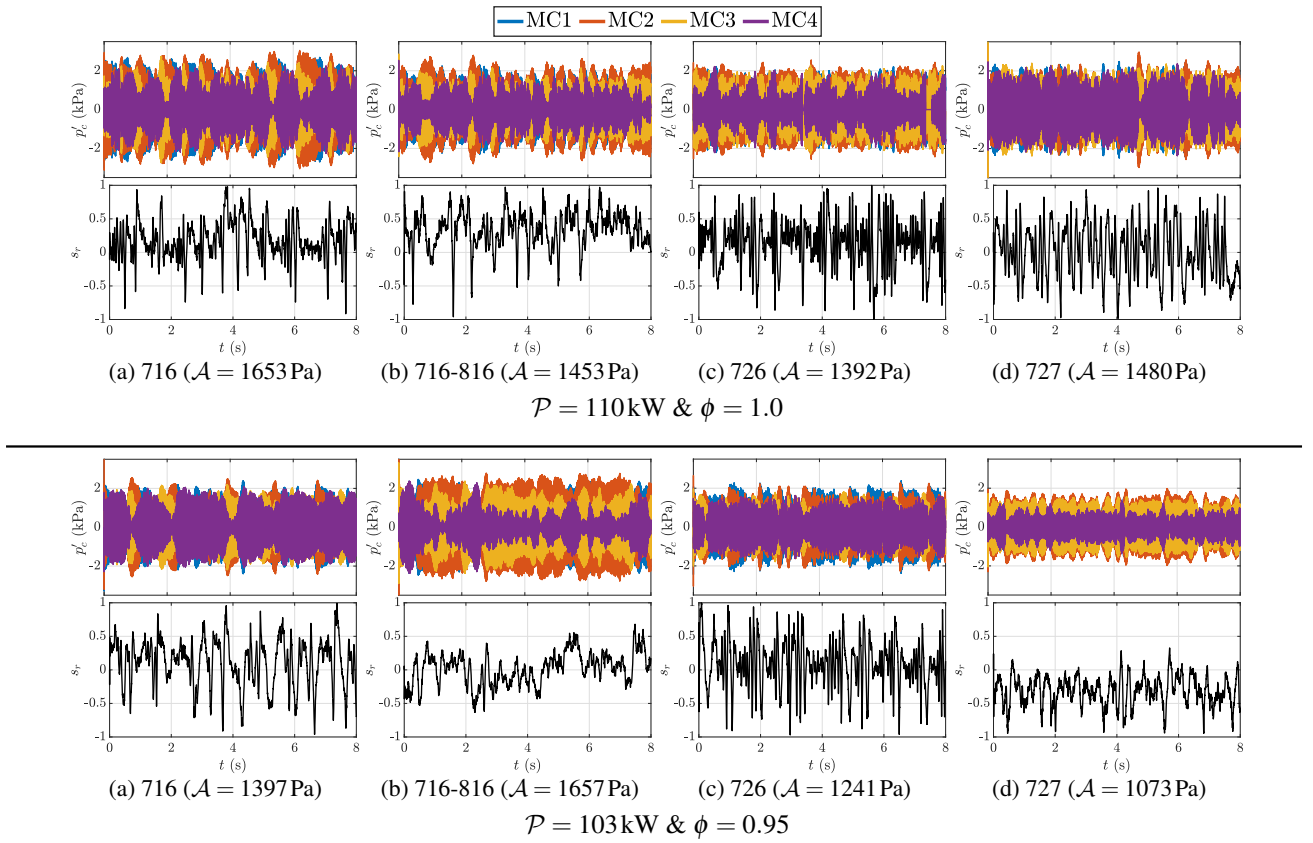

(a) 716 ($\mathcal{A} = 1653\,\text{Pa}$) (b) 716-816 ($\mathcal{A} = 1453\,\text{Pa}$) (c) 726 ($\mathcal{A} = 1392\,\text{Pa}$) (d) 727 ($\mathcal{A} = 1480\,\text{Pa}$)

$\mathcal{P} = 110\,\text{kW}$ & $\phi = 1.0$

(a) 716 ($\mathcal{A} = 1397\,\text{Pa}$) (b) 716-816 ($\mathcal{A} = 1657\,\text{Pa}$) (c) 726 ($\mathcal{A} = 1241\,\text{Pa}$) (d) 727 ($\mathcal{A} = 1073\,\text{Pa}$)

$\mathcal{P} = 103\,\text{kW}$ & $\phi = 0.95$

FIGURE 3: Time evolution of chamber pressure p_c' (MC1 to MC4) and spinratio s_r for the different swirlers. Two operating points are chosen from the instability map where strong instability is exhibited by the four swirler configurations. The pressure-spinratio set at the top corresponds to $\{\mathcal{P} = 110\,\text{kW}\ \&\ \phi = 1.0\}$, and the bottom set corresponds to $\{\mathcal{P} = 103\,\text{kW}\ \&\ \phi = 0.95\}$.

widen the region of instability. The amplitude map of 726 contains two discrete high-instability zones (red zones in Fig 2(c) left), one occurring at higher power and slightly richer conditions and the other occurring at lower power and leaner equivalence ratio. Swirlers 716 and 727 however exhibit continuous high-instability zones at higher equivalence ratios and are always stable at the lowest power. All the swirlers are stable at the lowest equivalence ratio, irrespective of the thermal power.

On comparing the frequency maps, swirlers 716 and 727 have similar values. But with 726, the frequencies are nearly 15 Hz higher than that of the other two swirlers. The operating point where the instability frequency is the highest occurs at $\mathcal{P} = 118\,\text{kW}$ and close to stoichiometry. As expected, this region features the highest value of adiabatic flame temperature resulting in the highest instability frequency.

It is also interesting to probe particular points on the stability maps to compare the variations exhibited by the different swirlers. Two points are chosen, corresponding to $\{\mathcal{P} = 110\,\text{kW}\ \&\ \phi = 1.0\}$ and $\{\mathcal{P} = 103\,\text{kW}\ \&\ \phi = 0.95\}$, where all the three swirlers exhibit strong instabilities. The pressure-time evolution is traced for four chamber microphones and is shown in the top rows of Fig. 3, whereas the bottom rows of this figure show the spin ratio evolution for half of the total acquisition period. From the pressure traces, it can be observed that, although an overall limit cycle envelope can be traced, these instabilities do not exhibit a clean limit cycle but rather feature small and random bursts (quasi-limit cycle operation), which depend on the operating point. The spin ratio evolution shows that the instabilities are degenerate and constantly switch between standing and spinning modes. Such modal behavior has been previously observed in the LES study in [10], and in experimental investigations in annular combustors [5, 33]. Swirler 716 exhibits an almost similar spin ratio evolution between the two operating points, fluctuating between standing and the two spinning modes. Swirler 726 exhibits similar spin ratio evolution at the two operating points and features rapid oscillation between the different modes but centered at the standing mode. Swirler 727 exhibit a completely different evolution between the two points. At $\{\mathcal{P} = 110\,\text{kW}\ \&\ \phi = 1.0\}$, s_r rapidly oscillates between the standing and two spinning modes, whereas, at $\{\mathcal{P} = 110\,\text{kW}\ \&\ \phi = 0.95\}$, it only

oscillates between standing and clockwise spinning mode.

4 INSTABILITY BEHAVIOR WITH CO- AND COUNTER-ROTATING SWIRLERS

It is now interesting to compare the combustion dynamics in a configuration where all the swirlers impart clockwise rotation (all are of 716-type, referred as CR), and a configuration where clockwise and counterclockwise rotating swirlers are alternatively placed (716-816, referred as CCR). This analysis will help identify the role of bulk swirl along the annular chamber that is induced when all the swirlers rotate in the same direction. A similar study was carried out previously by Worth & Dawson [5] on an annular combustor using a different class of injectors comprising a bluff-body stabilizer and featuring a lower swirl number. In the present experiments, the bulk rotation would be oriented in the clockwise direction along the outer wall of the annulus, whereas it would be oriented in the anticlockwise direction along the inner side of the annulus. This would be canceled out in a configuration where co- and counter-rotating swirlers are alternatively placed. In addition, a complete CR swirler arrangement would result in a shear velocity zone between two adjacent injectors due to the opposite direction of the swirling velocity.

The stability maps in Fig. 2(a) & (b) right show that the instability frequency does not differ between the cases. This is expected, as changing the swirl direction does not change the overall temperature environment in the chamber, which in turn is reflected in the instability frequency. On the other hand, some changes appear in the amplitude stability map (Fig. 2(a) & (b) left) which appears to be shifted towards lower thermal power and a lower equivalence ratio for CCR arrangement compared to CR arrangement. This can be better appreciated by probing the point where the maximum instability amplitude occurs for the two configurations. The maximum amplitude of instability is $\mathcal{A}_{\max} = 1673\,\mathrm{Pa}$ for CR arrangement which is slightly lower compared to CCR combination of $\mathcal{A}_{\max} = 1775\,\mathrm{Pa}$. For the CR configuration, this corresponds to a thermal power of $\mathcal{P} = 110\,\mathrm{kW}$ and $\phi = 1.05$, whereas for the CCR configuration, this occurs at a lower thermal power of $\mathcal{P} = 103\,\mathrm{kW}$ and a lower equivalence ratio of $\phi = 1.0$. On comparing the pressure-time series evolution in Fig. 3, one observes that similar to full CR, the CCR arrangement also exhibits a quasi-limit cycle mode of operation with intermittent bursts.

Previous studies on annular combustors [5, 10], indicate that when all the swirlers impart rotation in the same direction (CR), the bulk swirl imposes a slow rotational motion to the $s_r = 0$ standing mode rather than making it remain stationary. Worth and Dawson [5] also find that, in a configuration where alternate anticlockwise and clockwise swirlers are placed (CCR), there is a statistical preference towards a standing mode compared to the case where all swirlers induce rotation in the same direction. In the latter case, mode preference depended on the operating condition. To see if this is verified in the present configuration, one may examine the distribution of spin ratio plotted in Fig. 4 for the CR and CCR configurations at four thermal powers ($\mathcal{P}$: 118, 110, 103, 99 kW) and at two equivalence ratios (0.9 and 1). The spin ratio histogram is not available for the CCR combination at 99 kW and $\phi = 1$, as MICCA-Spray is stable at this operating point for this configuration. One observes from the histograms that most of the spin ratio distributions resemble a Gaussian random process with a mean and standard deviation that depends on the operating point. The preferred operating mode be roughly deduced from the mean spin ratio $\overline{s_r}$, shown as a vertical red line in Fig. 4. This mean spin ratio lies in the positive zone irrespective of the configuration or is close to $s_r = 0$. This indicates that the statistical preference is mostly either a standing mode or anticlockwise spinning mode but not a clockwise spinning mode except for the CR configuration at 99 kW and $\phi = 0.9$ where the distribution inclines towards clockwise spinning mode. At the highest thermal power (118 kW), one observes a definite pattern where the full CR combination has a narrow distribution inclined towards the counterclockwise zone without ever reaching the clockwise spinning zone, while the CCR combination has a wider distribution spanning the full range of spin ratios. This might be attributed to an effect of the bulk swirl, but one observes that the other operating points feature a relatively broad distribution for a CR configuration as well (for example, see Fig. 4(c),(i) & (j)). Contrary to the observation in [5], on comparing the two configurations at eight operating points, one observes that, in the present case, there is no statistical preference for a particular mode. One may generally say that a configuration with alternate co- and counter-rotating swirlers exhibits a wider distribution of spin ratios compared to a fully co-rotating swirler configuration where the distribution is mostly but not always narrower. Thus, one cannot infer that the presence of a bulk swirl determines the nature of the coupling mode.

5 FLAME DESCRIBING FUNCTIONS AND THEIR IMPACT

It is natural to see whether flame describing functions (FDFs) can be used to analyze the differences in unstable behavior observed in MICCA-Spray with the various swirler units. The FDFs are determined in a single-injector combustor, namely SICCA-Spray, that represents one sector of the MICCA-Spray annular combustor. Studying these injectors on a simplified setup allows to perform specific diagnostics and measurements in order to understand the differences observed in MICCA-Spray. This analysis is carried out at one operating point selected from the MICCA-Spray stability map, which is marked as a black star in Fig. 2. At this operating point, the annular combustor operates at a thermal power of $\mathcal{P} = 103\,\mathrm{kW}$ and equivalence ratio of $\phi = 0.85$. The corresponding thermal power of SICCA-Spray is $\mathcal{P}_{\mathrm{sicca}} = 6.4\,\mathrm{kW}$. The different swirlers of the higher-swirl group

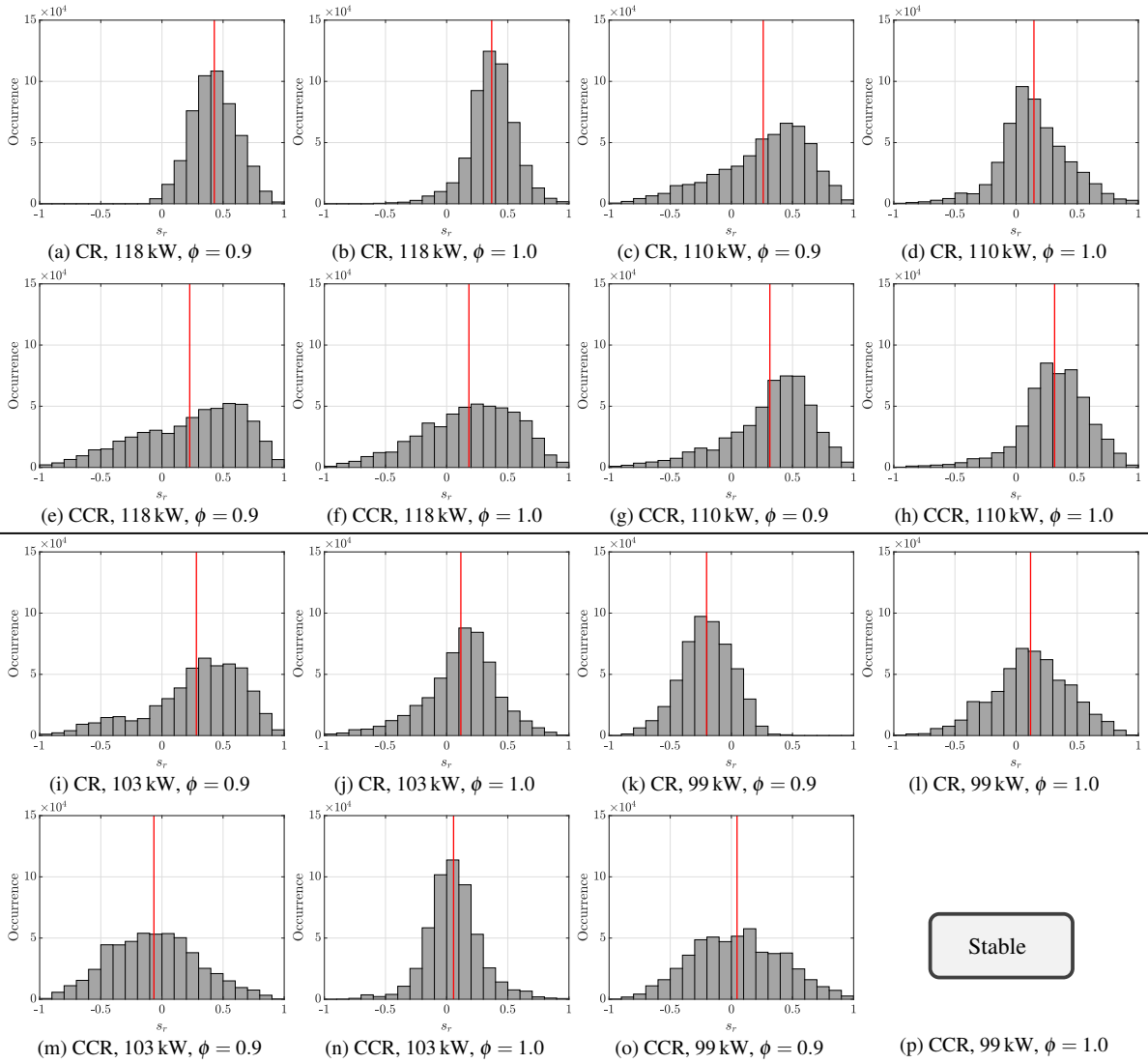

(a) CR, 118 kW, $\phi = 0.9$ (b) CR, 118 kW, $\phi = 1.0$ (c) CR, 110 kW, $\phi = 0.9$ (d) CR, 110 kW, $\phi = 1.0$

(e) CCR, 118 kW, $\phi = 0.9$ (f) CCR, 118 kW, $\phi = 1.0$ (g) CCR, 110 kW, $\phi = 0.9$ (h) CCR, 110 kW, $\phi = 1.0$

(i) CR, 103 kW, $\phi = 0.9$ (j) CR, 103 kW, $\phi = 1.0$ (k) CR, 99 kW, $\phi = 0.9$ (l) CR, 99 kW, $\phi = 1.0$

(m) CCR, 103 kW, $\phi = 0.9$ (n) CCR, 103 kW, $\phi = 1.0$ (o) CCR, 99 kW, $\phi = 0.9$ (p) CCR, 99 kW, $\phi = 1.0$

FIGURE 4: Histogram of spin ratio occurrence comparing a configuration where all the swirlers are co-rotating (CR) and a configuration where co- and counter-rotating (CCR) swirlers are alternatively placed. The red vertical line corresponds to the mean spin ratio $\overline{s_r}$. The results are presented at four thermal powers and two equivalence ratios at each point, except for CCR arrangement at $\mathcal{P} = 99\,\text{kW}$ & $\phi = 1$ as MICCA-Spray is stable at this point.

all exhibit similar instability amplitudes ($\approx 800\,\text{Pa}$) in MICCA-Spray at the chosen point. The experimental setup used for this purpose is shown in Fig. 1(c) and is described in some previous investigations [7, 30, 31]. The rig consists of a cylindrical quartz chamber with an inner diameter 69 mm allowing optical access to the flame region and is operated with the same injectors as MICCA-Spray. Although the wall-bounded flames of SICCA-Spray cannot be exactly used to represent the flames of MICCA-Spray, which exhibit flame-flame interaction, it is concluded in a parallel investigation that they reproduce the flame dynamics in MICCA-Spray to a reasonable extent [34]. It is logical to first examine the flame shapes under steady conditions, before discussing the flame response in terms of FDFs.

5.1 Flame shapes formed by the different swirlers

Flame images displayed in Fig. 5 are recorded when the SICCA-Spray combustor is in steady state operation. Each image is obtained by averaging 30 frames and applying an Abel inversion to the data gathered by an intensified CCD camera fitted with an OH* filter (centered at 310 nm).

The overall flame shapes formed by the lower-swirl injectors

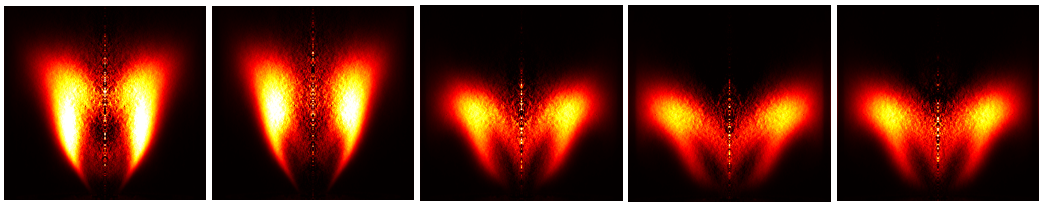

(a) 707 (b) 712 (c) 716 (d) 726 (e) 727

FIGURE 5: Flame images showing OH* chemiluminescence captured in SICCA-Spray under stable conditions. An Abel inversion is applied to the averaged images captured by the camera and are displayed in false colors. $\mathcal{P}_{\text{sicca}} = 6.4\,\text{kW}$ and $\phi = 0.85$.

notably differ from those formed by the higher-swirl units. The lower-swirl devices (707 and 712) form "V" shape flames that are narrower and longer. Such flames would result in lower interaction with the neighboring flames in MICCA-Spray. Between 707 and 712, the flames differ in the distribution of chemiluminescence intensity; while 707 has a more uniform distribution in the flame wings, 712 features a more concentrated chemiluminescence intensity close to the tip.

The higher-swirl units form "M" flames that are generally wider resulting in augmented flame-flame interaction in MICCA-Spray. Some minor differences exist between the swirlers of this category. The flame wing angle is lower for 716 compared to the other two swirlers (726 and 727), probably because this unit has a lower swirl number. A modest difference exists between 726 and 727 in the two central branches, which are seen to merge at a larger distance from the outlet for 727 compared to 726. This is possibly linked to the difference in pressure drop values. Differences in mean flame shapes can be expected to influence the flame response to incoming disturbances, as confirmed in what follows.

5.2 Measurement of flame describing function

The flame response to external acoustic modulations is obtained in the SICCA-Spray combustor in terms of a flame describing function (FDF). In the absence of equivalence ratio fluctuations, the FDF is given by:

$$\mathcal{F} = \frac{\dot{Q}'/\overline{\dot{Q}}}{\dot{q}_v'/\overline{\dot{q}_v}} \tag{3}$$

where $\dot{Q}'/\overline{\dot{Q}}$ represent the relative fluctuations in heat release rate of the flame and $\dot{q}_v'/\overline{\dot{q}_v}$ represent the relative fluctuations in volume flow rate. The assumption that equivalence ratio fluctuations are negligible is verified in [31] for the injectors considered in the present study. The heat release rate fluctuations can then be measured by obtaining the intensity of chemiluminescence emitted by excited radicals such as OH* or CH*. While this is well validated for premixed flames, the case of spray flames is complicated as they may feature spatial inhomogeneities in equivalence ratio. This aspect is considered in [31] where it is concluded that these injectors behave in a quasi-premixed fashion due to the recessed position of the atomizer. Thus, for the present spray flames, chemiluminescence intensity can be used as an indicator of heat release rate. A photomultiplier fitted with an OH* filter centered at 308 nm records the mean and fluctuating light intensities $I'(\text{OH*})/\overline{I(\text{OH*})}$ from the flame which approximately represents the relative heat release rate fluctuations $\dot{Q}'/\overline{\dot{Q}}$.

The relative fluctuations in volume flow rate $\dot{q}_v'/\overline{\dot{q}_v}$ is often replaced by the relative velocity fluctuations $u'/\overline{u}$ for ease of measurement. Such a substitution is valid as long as the measurement is carried out in a region where the relative velocity fluctuations match the relative volumetric flow rate fluctuations. In several studies, velocity fluctuations are measured in the plenum. However, this lumps together the injector and flame responses and may not be appropriate when the injector is only weakly transparent to acoustic modulations [31]. It is then preferable to measure the relative velocity fluctuations at a point in the chamber where they are equivalent to relative volumetric flow rate fluctuations. In the present case, the measurement points are chosen to be $r = 3.5\,\text{mm}$ for the swirlers in the lower-swirl category (707 and 712) and at $r = 4\,\text{mm}$ for the swirlers in the higher-swirl category (716, 726, 727) from the center of the injector and at a height of $h = 2.5\,\text{mm}$ above the backplane. The axial velocity fluctuations are measured with a Dantec Dynamics 2-component phase Doppler particle analyzer (PDPA) system operating in laser Doppler anemometry mode and making use of the heptane droplets in the spray. This is adequate because the droplet size at the measurement point does not exceed a mean diameter of 8 µm and the droplets, therefore, follow the air flow well in the frequency range of interest.

The two driver units mounted at the bottom of SICCA-Spray are modulated at different frequencies and amplitudes to obtain the gain G and phase φ of FDF at different levels of relative velocity fluctuations $u'/\overline{u}$ at the injector outlet. The FDFs are shown in Fig. 6 for the five swirling injectors considered in this study. The FDFs for the lower-swirl category (Fig. 6 (a) &

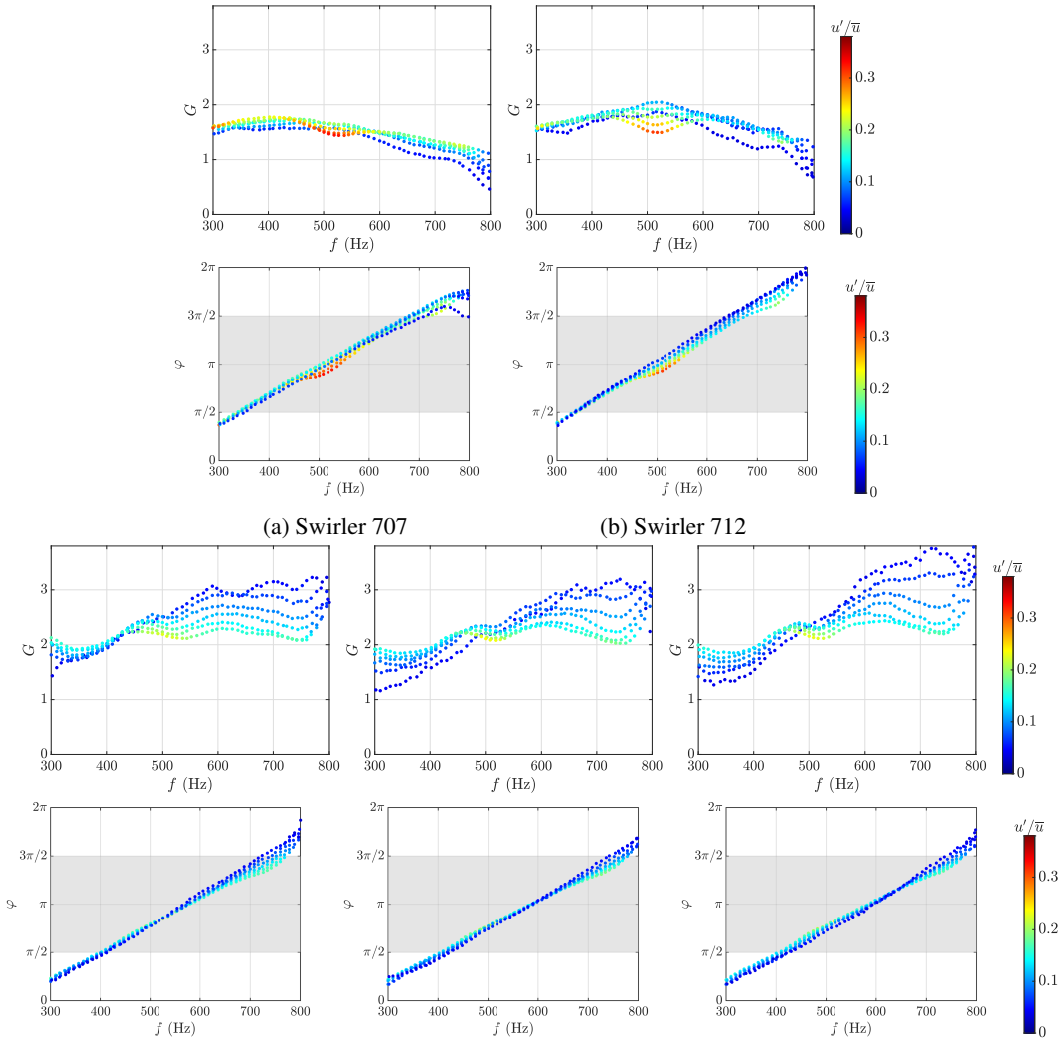

(a) Swirler 707 (b) Swirler 712

(c) Swirler 716 (d) Swirler 726 (e) Swirler 727

FIGURE 6: Flame describing function represented in terms of gain G and phase φ at different levels of relative velocity fluctuation $u'/\overline{u}$ and shown for the five swirlers considered. The gray bands on the phase diagrams indicate the tentative unstable bands.

(b)) notably differ in both gain and phase from the FDFs of the higher-swirl category (Fig. 6 (c), (d), & (e)). However, the FDFs are quite similar when the swirlers belong to the same category. On comparing the swirlers 707 and 712 (Fig. 6 (a) & (b), top), it can be observed that the overall trend in gain is preserved with some minor differences. While the gain of 707 evolves almost linearly with the velocity fluctuation levels, 712 exhibits mild variations in gain with respect to velocity fluctuation level close to 500 Hz in the tested amplitude range. The gain for swirler 707 features a plateau until 600 Hz beyond which there is a steady drop. For swirler 712, the gain mildly increases in the low frequency range ($<$ 600 Hz) and falls beyond that frequency. Similarly, the gains of the swirlers 716, 726, and 727 exhibit the same overall behavior, the gain rises until around 600 Hz, beyond which it nearly reaches a plateau. In the low frequency zone, the gain of 716 is almost independent of velocity fluctuation level but then exhibits substantial sensitivity to the excitation level beyond 500 Hz. The other two swirlers (726 and 727) exhibit a weak nonlinearity, first at the lower velocity fluctuation amplitudes and below 500 Hz, but this becomes more pronounced beyond this limit, similar to the case of swirler 716. For the same level of amplifier input voltages delivered to the driver units of SICCA-Spray, 707 reaches the highest level of velocity fluctuations, with $u'/\overline{u} \approx 37\%$ at a frequency of around 500 Hz. This level is slightly lower for 712 at 31%, whereas the swirlers in the higher-swirl category feature a maximum level of about

23%. These limitations in relative modulation levels may be attributed to the low pressure drops of 707 and 712. The swirlers in the higher-swirl category also feature the highest pressure drop values offering higher resistance to the incoming acoustic disturbances.

The phase of the FDF is almost exclusively linear for all of the swirlers in the amplitude range tested. A mild nonlinearity is observed around 500 Hz for 707, beyond 500 Hz for 712, and beyond 700 Hz for the higher-swirl units. The phase of the FDF essentially depends on the swirler category. In general, the higher-swirl units have similar phase functions, whereas the lower-swirl devices differ in their phase characteristics beyond 630 Hz. Although the differences are well pronounced between the two swirler categories in the gain, the differences in the phase of FDF are less apparent.

5.3 Instability prediction using FDFs

The FDF framework allows for a reasonable prediction of instabilities observed in MICCA-Spray as demonstrated in [12]. For injectors that are weakly transparent to acoustic waves, like the ones considered here, it has been shown in [31] that a low-order model may be used to predict instabilities of SICCA-Spray. The model consists of imposing an impedance ζ at the injector outlet, the phase of which determines "unstable bands", and an experimentally determined FDF $\mathcal{F}$ to represent the flame dynamics. From the model, one may infer a qualitative interpretation of observations made in the annular system.

The model yields unstable bands, which can be represented on the FDF phase diagram. If the phase of the FDF at a particular frequency falls within this band, then one can predict a "potential instability" at this frequency. The location of this unstable band is predominantly decided by the phase of the impedance φ_ζ at the injector outlet. In addition, one also obtains a growth rate for the instability, which directly depends on the gain of FDF. If this growth rate is greater than the damping imposed by the system, then it can be concluded that a particular operating point will be "definitely unstable" in MICCA-Spray. Using this simplified representation of the injector and FDF, an attempt is made to predict the instabilities of the MICCA-Spray combustor. It has been shown in [31] that for an acoustically weakly transparent injector, the impedance measured at the injector outlet takes a phase φ_ζ in the range $[3\pi/4, \pi]$ for frequencies lying between 300 and 600 Hz. This result is also obtained in [35] using a similar injector placed in a linear multi-injector test rig and submitted to transverse acoustic perturbations. One may then tentatively assume, in the absence of information on the definite injector impedance in the annular configuration, that the unstable band lies in the range between $[\pi/2, 3\pi/2]$, and place this band in the phase diagrams shown in Fig. 6 (marked as gray region). Noting that the instabilities in MICCA-Spray have oscillation eigenfrequencies lying between 750 and 832 Hz, one can see that the phases for 707 and 712 cross the $3\pi/2$ upper limit of the unstable band at 700 Hz and 650 Hz respectively. This clearly indicates that the two lower-swirl units will not give rise to 1A1L instability in MICCA-Spray. For the three swirlers in the higher-swirl group, the phase of the instability band crosses the $3\pi/2$ limit at $\approx$ 790 Hz at the highest level of velocity fluctuations ($u'/\overline{u} \approx 15\%$ in Fig. 6 (c-e) bottom). This crossing frequency is close to the 1A1L eigenfrequency providing a positive growth rate. This means that these swirlers might give rise to an instability and that their crossing frequency would then increase as the amplitude grows, while the phase would continue to be reduced and stay within the unstable band in Fig. 2 so that the oscillation corresponding to 726 would finally reach a limit cycle at a frequency of 832 Hz. Of course this is only a tentative scenario, since there is no information beyond 800 Hz and also because the unstable band has been placed in the range $[\pi/2, 3\pi/2]$.

The other aspect of the model is to have a sufficient growth rate level, which can be roughly estimated based on the gain of FDF. From the gain plots in Fig. 6, a large difference is observed between the two swirl categories. For the lower-swirl group, the gain takes a decreasing trend between 750 and 832 Hz and passes below 1. Whereas, for the higher-swirl category, the gain increases in this zone and is about two times higher than that of the lower-swirl category. The three swirlers in the higher-swirl category also possess a similar value of FDF gain ($G_{\text{average}} \approx 2.8$) which is reflected as similar amplitudes in the annular combustor at this operating point ($\mathcal{A} \approx 800$ Pa). This partially explains the reason for the swirlers in the higher-swirl category being unstable in MICCA-Spray, whereas the lower-swirl category swirlers are always stable.

6 CONCLUSION

To identify swirler effects on azimuthal combustion instabilities, systematic experiments were carried out on a lab-scale annular combustor equipped with sixteen injectors. The present investigation reports results obtained with five different swirlers that may be qualified as weakly transparent to acoustic waves. Their swirl numbers range from 0.59 to 0.74 with relatively high pressure drop coefficients. The swirlers are categorized based on the swirl number values into lower-swirl (swirlers 707 and 712) and higher-swirl (swirlers 716, 726, 727) groups with variations in pressure drops within each category. The swirlers in the lower-swirl group also have comparatively lower pressure drops. Experiments are carried out with liquid heptane at five thermal power and six global equivalence ratio levels (30 operating points) for each swirler. The data are then used to plot stability maps which reveal that the swirler type has a notable influence on the stability characteristics of the system. One observes that:

- None of the swirlers in the lower-swirl category feature

an instability at any of the thirty operating points tested. In contrast, all the swirlers in the higher-swirl category give rise to azimuthal instabilities.

- The transition to an unstable mode is mostly determined by the swirl number through its effect on flame structure. The pressure drop contributes to further variations in amplitude and frequency of oscillation.
- On comparing the swirlers in the higher-swirl category, a higher pressure loss value appears to be associated with wider instability regions and higher oscillation frequency.
- The evolution of the spin ratio reveals that the modes are degenerate, and constantly fluctuate between standing and spinning modes, an observation similar to [5, 10].

An additional case, where alternatively-placed co-rotating and counter-rotating (CCR) swirlers, is compared with the standard arrangement, where all the swirlers are co-rotating (CR), to reveal possible effects of mean bulk swirl on instabilities. It is seen that:

- Compared to the CR arrangement, the stability map for the CCR arrangement is shifted towards lower thermal power and lower equivalence ratio.
- When the mean bulk swirl is absent, the spin ratio distribution does not feature a statistical preference to standing or spinning mode.
- In some cases, the CCR configuration promotes a broader distribution of spin ratios centered around the standing mode ($s = 0$) while the CR setup appears to favor counterclockwise spinning modes.

Flame shapes and flame describing functions (FDFs) measured in a single-injector combustor, namely SICCA-Spray representing one sector of MICCA-Spray, are employed to interpret the differences in behavior observed in the annular system at one operating point. Results show that:

- The flame shapes obtained under stable conditions are distinct for each swirler category. Swirlers in the lower-swirl category generally take a "V" shape, whereas the swirlers in the higher-swirl category take an "M" shape.
- The dynamical response of the flames represented in terms of an FDF also distinctly depend on the swirler category.

An attempt is made to qualitatively interpret instability observations in the annular combustor by making use of a low-order model combining the FDFs and impedance at the swirler outlet [31]. For the lower-swirl injector, one infers that the phase lies outside the instability band in the frequency range of the 1A1L mode. In the higher-swirl case, the phase is near the band's upper boundary in the frequency range of the 1A1L mode, and the gain takes larger values that are about twice those of the lower-swirl units. These two features would then promote the growth of instability. As the gain decreases with the amplitude of velocity oscillations, this will lead to a limit cycle.

ACKNOWLEDGMENT

This work was supported by the European Union's Horizon 2020 research and innovation programme, Annulight with grant agreement no. 765998.

REFERENCES

[1] Mongia, H. C., Held, T., Hsiao, G., and Pandalai, R., 2003. "Challenges and progress in controlling dynamics in gas turbine combustors". *J. Propul. Power,* ***19***(5).

[2] Lieuwen, T. C., and Yang, V., 2005. "Combustion instabilities in gas turbine engines: operational experience, fundamental mechanisms, and modeling". *Am. Inst. Aeronaut. Astronaut.*

[3] Poinsot, T., 2017. "Prediction and control of combustion instabilities in real engines". *Proc. Combust. Institute,* ***36***(1).

[4] Staffelbach, G., Gicquel, L., Boudier, G., and Poinsot, T., 2009. "Large eddy simulation of self excited azimuthal modes in annular combustors". *Proc. Combust. Inst.,* ***32***(2), pp. 2909–2916.

[5] Worth, N. A., and Dawson, J. R., 2013. "Modal dynamics of self-excited azimuthal instabilities in an annular combustion chamber". *Combust. Flame,* ***160***(11), pp. 2476–2489.

[6] Prieur, K., Durox, D., Schuller, T., and Candel, S., 2017. "A hysteresis phenomenon leading to spinning or standing azimuthal instabilities in an annular combustor". *Combust. flame,* ***175***, pp. 283–291.

[7] Rajendram Soundararajan, P., Vignat, G., Durox, D., Renaud, A., and Candel, S., 2021. "Effect of different fuels on combustion instabilities in an annular combustor". *J. Eng. Gas Turb. Power,* ***143***(3), p. 031007.

[8] Aguilar, J. G., Dawson, J., Schuller, T., Durox, D., Prieur, K., and Candel, S., 2021. "Locking of azimuthal modes by breaking the symmetry in annular combustors". *Combust.Flame,* ***234***, p. 111639.

[9] Wolf, P., Balakrishnan, R., Staffelbach, G., Gicquel, L. Y., and Poinsot, T., 2012. "Using LES to study reacting flows and instabilities in annular combustion chambers". *Flow, Turbulence Combus.,* ***88***(1), pp. 191–206.

[10] Wolf, P., Staffelbach, G., Gicquel, L. Y., Müller, J.-D., and Poinsot, T., 2012. "Acoustic and large eddy simulation studies of azimuthal modes in annular combustion chambers". *Combust. Flame,* ***159***(11), pp. 3398–3413.

[11] Pankiewitz, C., and Sattelmayer, T., 2003. "Time domain simulation of combustion instabilities in annular combustors". *J. Eng. Gas Turb. Power,* ***125***(3), pp. 677–685.

[12] Laera, D., Schuller, T., Prieur, K., Durox, D., Camporeale, S. M., and Candel, S., 2017. "Flame describing function analysis of spinning and standing modes in an annular

combustor and comparison with experiments". *Combust. Flame,* ***184***, pp. 136–152.

[13] Ghirardo, G., and Juniper, M. P., 2013. "Azimuthal instabilities in annular combustors: standing and spinning modes". *Proc. R. Soc. A: Math., Phys. Eng. Sci.,* ***469***(2157), p. 20130232.

[14] Parmentier, J.-F., Salas, P., Wolf, P., Staffelbach, G., Nicoud, F., and Poinsot, T., 2012. "A simple analytical model to study and control azimuthal instabilities in annular combustion chambers". *Combust. Flame,* ***159***(7).

[15] Steele, R. C., Cowell, L. H., Cannon, S. M., and Smith, C. E., 2000. "Passive control of combustion instability in lean premixed combustors". *J. Eng. Gas Turb. Power,* ***122***(3), pp. 412–419.

[16] Krishnan, A., Sujith, R., Marwan, N., and Kurths, J., 2021. "Suppression of thermoacoustic instability by targeting the hubs of the turbulent networks in a bluff body stabilized combustor". *J. Fluid Mech.,* ***916***.

[17] Noiray, N., Durox, D., Schuller, T., and Candel, S., 2009. "Dynamic phase converter for passive control of combustion instabilities". *Proc. Combust. Inst.,* ***32***(2).

[18] Annaswamy, A. M., and Ghoniem, A. F., 2002. "Active control of combustion instability: Theory and practice". *IEEE Control Systems Magazine,* ***22***(6), pp. 37–54.

[19] Huang, Y., and Yang, V., 2009. "Dynamics and stability of lean-premixed swirl-stabilized combustion". *Prog. Energy Combust. Sci.,* ***35***(4), pp. 293–364.

[20] Candel, S., Durox, D., Schuller, T., Bourgouin, J.-F., and Moeck, J. P., 2014. "Dynamics of swirling flames". *Ann. Rev. Fluid Mech.,* ***46***, pp. 147–173.

[21] Worth, N. A., and Dawson, J. R., 2013. "Self-excited circumferential instabilities in a model annular gas turbine combustor: Global flame dynamics". *Proc. Combust. Inst.,* ***34***(2), pp. 3127–3134.

[22] Bourgouin, J.-F., Durox, D., Moeck, J. P., Schuller, T., and Candel, S., 2015. "Characterization and modeling of a spinning thermoacoustic instability in an annular combustor equipped with multiple matrix injectors". *J. Eng. Gas Turb. Power,* ***137***(2).

[23] Bourgouin, J.-F., Durox, D., Moeck, J., Schuller, T., and Candel, S., 2015. "A new pattern of instability observed in an annular combustor: The slanted mode". *Proc. Combust. Inst.,* ***35***(3), pp. 3237–3244.

[24] Steinberg, A. M., Boxx, I., Stohr, M., Meier, W., and Carter, C. D., 2012. "Effects of flow structure dynamics on thermoacoustic instabilities in swirl-stabilized combustion". *AIAA journal,* ***50***(4), pp. 952–967.

[25] Paschereit, C. O., Gutmark, E., and Weisenstein, W., 2000. "Excitation of thermoacoustic instabilities by interaction of acoustics and unstable swirling flow". *AIAA journal,* ***38***(6).

[26] Huang, Y., and Yang, V., 2005. "Effect of swirl on combustion dynamics in a lean-premixed swirl-stabilized combustor". *Proc. Combust. Inst.,* ***30***(2), pp. 1775–1782.

[27] Komarek, T., and Polifke, W., 2010. "Impact of swirl fluctuations on the flame response of a perfectly premixed swirl burner". *J. Eng. Gas Turb. Power,* ***132***(6).

[28] Kim, K. T., 2016. "Combustion instability feedback mechanisms in a lean-premixed swirl-stabilized combustor". *Combust. Flame,* ***171***, pp. 137–151.

[29] Zhang, B., Shahsavari, M., Rao, Z., Yang, S., and Wang, B., 2021. "Thermoacoustic instability drivers and mode transitions in a lean premixed methane-air combustor at various swirl intensities". *Proc. Combust. Inst.,* ***38***(4).

[30] Vignat, G., Durox, D., Prieur, K., and Candel, S., 2019. "An experimental study into the effect of injector pressure loss on self-sustained combustion instabilities in a swirled spray burner". *Proc. Combust. Inst.,* ***37***(4), pp. 5205–5213.

[31] Rajendram Soundararajan, P., Durox, D., Renaud, A., Vignat, G., and Candel, S., 2022. "Swirler effects on combustion instabilities analyzed with measured FDFs, injector impedances, and damping rates". *Accepted in Combust. Flame*.

[32] Vignat, G., Durox, D., Renaud, A., and Candel, S., 2020. "High amplitude combustion instabilities in an annular combustor inducing pressure field deformation and flame blow off". *J. Eng. Gas Turb. Power,* ***142***(1).

[33] Bourgouin, J.-F., Durox, D., Moeck, J. P., Schuller, T., and Candel, S., 2013. "Self-sustained instabilities in an annular combustor coupled by azimuthal and longitudinal acoustic modes". In Proc. ASME Turbo Expo, p. V01BT04A007.

[34] Rajendram Soundararajan, P., Durox, D., Renaud, A., and Candel, S., 2022. "Comparison of flame describing functions measured in single and multiple injector configurations". In submitted to Proc. ASME Turbo Expo 2022.

[35] Patat, C., Baillot, F., Blaisot, J.-B., and Domingues, E., 2021. "Responses of lean swirling spray flames to acoustic pressure and transverse velocity perturbations". *Symp. Thermoacoust. Combust.: Ind. meets Acad.*, p. 8499.